Supplementary Material

Modeling thermodynamic properties of mixtures of $CO_2 + O_2$ in the Allam cycle by equations of state

Jens Staubach[1], *Gerhard Schwarz*[2], *Stephan Möbius*[2], *Hans Hasse*[1], *and Simon Stephan*[1]

[1)]Laboratory of Engineering Thermodynamics (LTD), RPTU Kaiserslautern, Kaiserslautern, 67633, Germany
[2)]KSB SE & Co. KGaA, Frankenthal, 67227, Germany
Simon.Stephan@rptu.de

November 4, 2023

The Supplementary Material for the publication contains the electronic spread sheet with the numeric values for the experimental data of the $CO_2 + O_2$ mixture used in this work. The pure component parameters for CO_2 and O_2 for the studied EOS are reported. The results for the phase equilibria at temperatures below $T < 273\,\mathrm{K}$ obtained from the EOS are reported. Furthermore, the overestimation of the critical point by molecular-based EOS and the performance on the 2^{nd}-order derivative properties by the different EOS is discussed. Additionally, deviation plots for the homogeneous state densities are shown for all ten studied EOS in the predictive and adjusted mode.

Electronic Spread Sheet

The electronic spread sheet includes two sheets *Information* and *Literature database*. The sheet *Information* gives the molar-mass of CO_2 and O_2 used for the unit conversion for the density. Additionally, the assignment of IDs used in the literature database to the corresponding sources is given. The columns of the sheet *Literature database* are the source ID, data type assignment (vapor phase, liquid phase, supercritical phase, vapor-liquid equilibrium), temperature $T\,/\,\mathrm{K}$, mass density $\rho\,/\,\mathrm{kg\ m^{-3}}$, molar density $\rho\,/\,\mathrm{mol\ l^{-3}}$, pressure $p\,/\,\mathrm{MPa}$, composition $x_{\mathrm{O_2}}\,/\,\mathrm{mol\ mol^{-1}}$ (in the case of vapor-liquid equilibrium liquid phase composition $x'_{\mathrm{O_2}}\,/\,\mathrm{mol\ mol^{-1}}$), vapor phase composition $x''_{\mathrm{O_2}}\,/\,\mathrm{mol\ mol^{-1}}$ (only for vapor-liquid equilibrium data points), isothermal compressibility $\beta\,/\,\mathrm{MPa^{-1}}$, speed of sound $w\,/\,\mathrm{m\ s^{-1}}$, and the outlier identifier.

Pure Component Parameters

The pure component model parameters for CO_2 and O_2 for the SRK, PR, PC-SAFT, PCP-SAFT, SAFT-VR Mie, polar soft-SAFT, BACKONE, and sCPA are given in Table S1 to S7, respectively. They were adopted from Refs. [1–9].

The attraction energy parameter a for the SRK, PR, and sCPA is derived by [10, 11]

$$a(T) = a_0 \left[1 + c_1 \left(1 - \sqrt{\frac{T}{T_\mathrm{c}}}\right)\right]^2, \tag{1}$$

where the parameters a_0 and c_1 are given in Table S7 for the sCPA. For the SRK EOS the parameter a_0 is calculated from

$$a_0^{\mathrm{SRK}} = 0.42747 \frac{R^2 T_\mathrm{c}^2}{p_\mathrm{c}}, \tag{2}$$

and for the PR EOS by

$$a_0^{\mathrm{PR}} = 0.45724 \frac{R^2 T_\mathrm{c}^2}{p_\mathrm{c}}, \tag{3}$$

with the universal gas constant R and the critical temperature T_c and critical pressure p_c given in Table S1. The parameter c_1 is calculated for the SRK EOS by

$$c_1^{\mathrm{SRK}} = 0.48 + 1.574\,\omega - 0.176\,\omega^2, \tag{4}$$

and for the PR EOS by

$$c_1^{\mathrm{PR}} = 0.37464 + 1.54226\,\omega - 0.26992\,\omega^2, \tag{5}$$

with the acentric factor given in Table S1. Additional, the co-volume parameter b is calculated for the SRK EOS by

$$b^{\mathrm{SRK}} = 0.08664 \frac{RT_\mathrm{c}}{p_\mathrm{c}}, \tag{6}$$

and for the PR by

$$b^{\mathrm{PR}} = 0.07780 \frac{RT_\mathrm{c}}{p_\mathrm{c}}. \tag{7}$$

The size parameter σ used in the mixing rule of the molecular-based EOS can be calculated for the BACKONE [12, 13] EOS by

$$\sigma^3 = \frac{0.1617}{N_\mathrm{A}\rho_0}, \tag{8}$$

where N_A is the Avogadro constant and ρ_0 is given in Table S6. The energy parameter $\varepsilon k_\mathrm{B}^{-1}$ is given by the simple relation

$$\varepsilon k_\mathrm{B}^{-1} = T_0. \tag{9}$$

Table S1 Pure component parameters for the Soave-Redlich-Kwong (SRK) [14] and Peng-Robinson (PR) [15] EOS for CO_2 and O_2. The parameters were adopted from Ref. [1]. The fourth to sixth column give the acentric factor ω, critical pressure p_c, and critical temperature T_c.

EOS	Reference	Substance	Parameters		
			ω	p_c / MPa	T_c / K
SRK and PR	[1]	CO_2	0.231	7.376	304.15
	[1]	O_2	0.019	5.08	154.77

Table S2 Pure component parameters for the PC-SAFT EOS [16] for CO_2 and O_2. The parameters were adopted from Ref. [4]. The fourth to sixth column give the chain length m, size parameter σ, and the energy parameter εk_B^{-1}.

EOS	Reference	Substance	Parameters		
			m	σ / Å	εk_B^{-1} / K
PC-SAFT	[4]	CO_2	2.6037	2.555	151.04
	[4]	O_2	1.1217	3.210	114.96

Table S3 Pure component parameters for the PCP-SAFT EOS [5, 16] for CO_2 and O_2. The parameters were adopted from Ref. [5] and Ref. [4]. The fourth to seventh column give the chain length m, size parameter σ, energy parameter εk_B^{-1}, and the quadrupole moment Q.

EOS	Reference	Substance	Parameters			
			m	σ / Å	εk_B^{-1} / K	Q / DÅ
PCP-SAFT	[5]	CO_2	1.5131	3.1869	163.33	4.4
	[4]	O_2	1.1217	3.210	114.96	-

Table S4 Pure component parameters for the SAFT-VR-Mie EOS [17] for CO_2 and O_2. The parameters were adopted from Ref. [6]. The fourth to seventh column give the chain length m, size parameter σ, energy parameter εk_B^{-1}, and the repulsive exponent λ_r.

EOS	Reference	Substance	Parameters			
			m	σ / Å	εk_B^{-1} / K	λ_r
SAFT-VR-Mie	[6]	CO_2	1.6936	3.0465	235.73	18.067
	[6]	O_2	1.4283	2.9671	81.476	8.9218

Table S5 Pure component parameters for the polar soft-SAFT EOS [18, 19] for CO_2 and O_2. The parameters were adopted from Ref. [7] and Ref. [8]. The fourth to eighth column give the chain length m, size parameter σ, energy parameter εk_B^{-1}, quadrupole moment Q, and the fraction of polar segments xp.

EOS	Reference	Substance	Parameters				
			m	σ / Å	εk_B^{-1} / K	Q / DÅ	xp
polar soft-SAFT	[7]	CO_2	1.571	3.166	166.5	4.4	0.333
	[8]	O_2	1.168	3.198	111.5	-	-

Table S6 Pure component parameters for the BACKONE EOS [9, 13] for CO_2 and O_2. The parameters were adopted from Ref. [9]. The fourth to seventh column give the anisotropy parameter α, characteristic density ρ_0, characteristic temperature T_0, and the reduced squared quadrupole moment Q^{*2}.

EOS	Reference	Substance	Parameters			
			α	ρ_0 / mol dm^{-3}	T_0 / K	Q^{*2}
BACKONE	[9]	CO_2	1.3919	10.549	291.28	2.181
	[9]	O_2	1.0244	13.629	154.58	-

Table S7 Pure component parameters for the sCPA EOS [11, 20] for CO_2 and O_2. The parameters were adopted from Ref. [2] and Ref. [3]. The fourth to eighth column give the parameter α, energy parameter a_0, co-volume parameter b, association energy parameter $\hat{\varepsilon}$, and association volume parameter $\hat{\beta}$. For the critical temperature T_c, cf. Eq. (1), $T_{c,CO_2} = 304.21\,\mathrm{K}$ [3] and $T_{c,O_2} = 154.58\,\mathrm{K}$ [3] were used. The association scheme 3B was used for CO_2.

EOS	Reference	Substance	Parameters				
			c_1	a_0 / L^2 bar mol^{-2}	b / L mol^{-1}	$\hat{\varepsilon}$ / bar L mol^{-1}	$\hat{\beta}$
sCPA	[2]	CO_2	0.6703	3.0558	0.0281	51.68	0.0411
	[3]	O_2	0.4754	1.39	0.0216	-	-

Mixture Model Adjustment

For the fitting of the phase equilibria, the algorithm was designed to check for reference data points for which the current model does not yield a phase split and these data points were removed from the cost function.

Vapor-Liquid Equilibrium

Figure S1 shows the calculated phase envelope by the studied EOS [5, 9, 11, 13–22] for three different temperatures in comparison to data from the literature [23–27]. Figure S2 shows the adjusted binary interaction parameter ξ_{CO_2,O_2} as a function of the temperature in the range $220\,\mathrm{K} \leq T \leq 420\,\mathrm{K}$.

For most EOS, the deviations of the phase envelope decrease when using the adjusted parameters, cf. Figure S1-bottom compared to Figure S1-top. The GERG-2008 EOS [21] with the adjusted binary interaction parameter underestimates the mixture critical point at low temperatures $T <= 253.15\,\mathrm{K}$, cf. Figure S1. Interestingly, the liquid phase mole fraction of CO_2 is underestimated for most EOS at low temperatures when using the adjusted parameters. This effect increases with stronger temperature dependency of the adjusted binary interaction parameter, cf. Figure S2. The temperature gradient $\frac{\mathrm{d}\xi}{\mathrm{d}T}$ increases from the SAFT-VR Mie > PC-SAFT > sCPA > PCP-SAFT EOS.

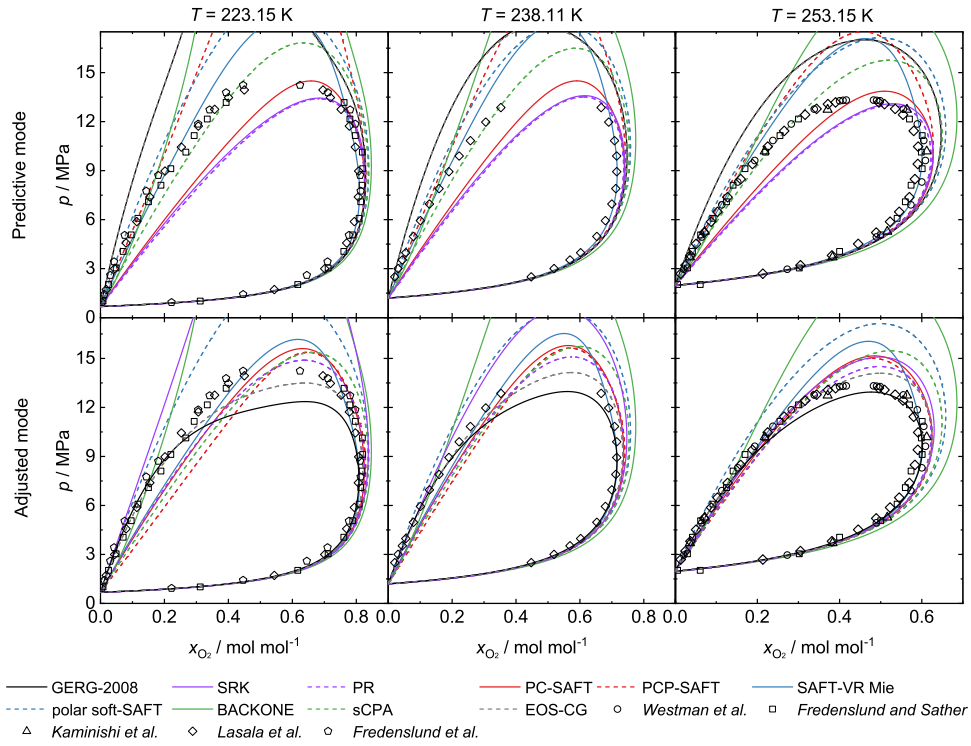

Fig. S1 Phase envelope of the system $CO_2 + O_2$ calculated by different EOS (lines) [5, 9, 11, 13–22] compared to literature data (symbols) [23–27]. Results from predictions based on pure component models (top) are compared to results that were obtained after adjusting binary parameters (bottom) to the training data. The GERG-2008 and EOS-CG results collapse to one line in the top figures (predictive mode).

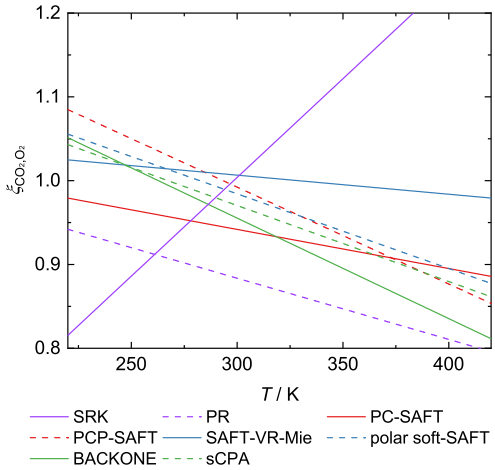

Fig. S2 Adjusted binary interaction parameter ξ_{CO_2,O_2} as a function of the temperature for cubic and molecular-based EOS.

Description of the Critical Point

Overall, EOS suffer from a poor description of the critical point, which is due to the underlying scaling behavior. This is not fixed by introducing a temperature-dependent binary interaction parameter, cf. Figure S1 and Figure 2 from the main body of this work. This overestimation of the critical point by EOS can be reduced by the inclusion of a renormalization group method, e.g. applied to the polar soft-SAFT in Ref. [28], the sCPA in Ref. [29], and the PC-SAFT in Ref. [30]. This leads to two to three additional parameters for each pure component and, additionally, the need to approximate an integral numerically during each calculation of the Helmholtz energy by the EOS. In this work, no renormalization group method was used. While the phase envelope prediction for mixtures and the prediction of $\rho(T, p, x)$ state points are improved by the renormalization group method, the speed of sound predictions are almost not effected in the case of CO_2 mixtures [29]. On the one hand the renormalization group method leads to improvements to the predictive calculations of the phase envelope, but on the other hand increased evaluation time of the EOS, more pure component parameters, and more complex mixing-rules.

2^{nd}-Order Derivative Properties

For the modeling of 2^{nd}-order derivative properties, the molecular-based EOS and the cubic EOS yield significantly larger deviations than the GERG-2008 EOS. Additional tests were carried out for adjusting the binary interaction parameters of the cubic and molecular-based EOS such that they yield a similar performance for the 2^{nd}-order derivative properties as the GERG-2008 EOS. We found that the binary interaction parameter ξ has to deviate significantly from unity such that unacceptable large deviations for the other properties are obtained. This was observed after the adjustment of the binary interaction parameters with equal weight to all objectives. Most likely, the deviations from the 2^{nd}-order derivatives property data are already introduced by the pure component models. This is shown in Figure S3 for the speed of sound, where the calculations from the GERG-2008 EOS are compared with the calculations from the PC-SAFT, PCP-SAFT, SAFT-VR Mie and the sCPA. The comparison shows the speed of sound for the binary mixture $CO_2 + O_2$ at $T = 278.15\,\text{K}$, cf. Figure S3 (left), and pure CO_2 at $T = 273.15\,\text{K}$, cf. Figure S3 (right). The mixture experimental data is described very well by the GERG-2008 EOS. The molecular-based EOS yield larger deviations from the experimental data, cf. Figure S3 (left). The results for the pure component speed of sound data at a slightly lower temperature are again described best by the GERG-2008, cf. Figure S3 (right). The trends of the deviations between the molecular-based EOS and the GERG-2008 is almost identical for pure CO_2 and the binary mixture of $CO_2 + O_2$ mixture. Therefore, to improve the prediction of the speed of sound in a significant way the pure component parameters of the molecular-based EOS need to be re-parametrized with speed of sound data included.

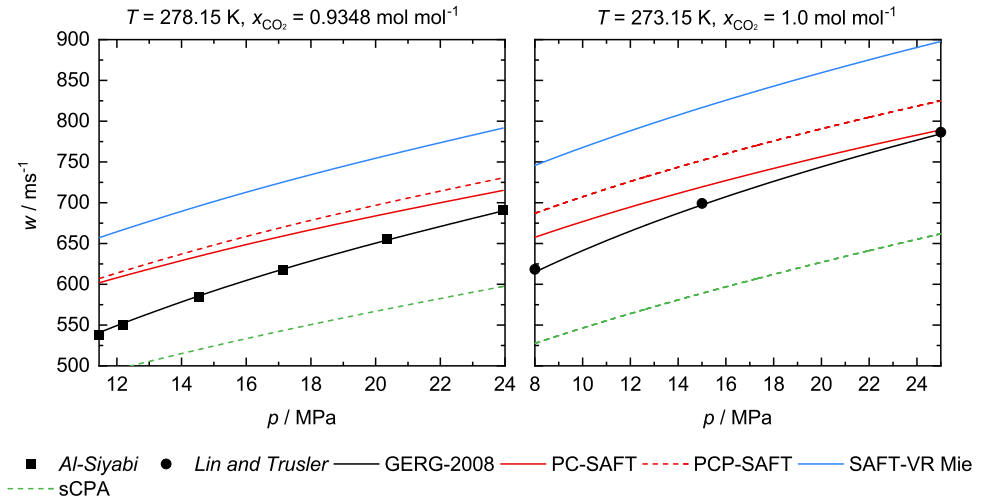

Fig. S3 Speed of sound w as a function of the pressure p at the temperature $T = 278.15\,\mathrm{K}$ for the binary $CO_2 + O_2$ mixture (left) and at $T = 273.15\,\mathrm{K}$ for pure CO_2 (right). The experimental data for the mixture are taken from *Al-Siyabi* [31] and for pure CO_2 from *Lin and Trusler* [32] (obtained in the original work by extrapolation from mixture experimental data). Experimental results are compared with the EOS [5, 11, 17, 20, 21, 33] used in the predictive mode.

Homogeneous State Density Deviations

Figure S4 and S5 show deviation plots for the homogeneous state densities for all ten studied EOS in the predictive mode and adjusted mode, respectively.

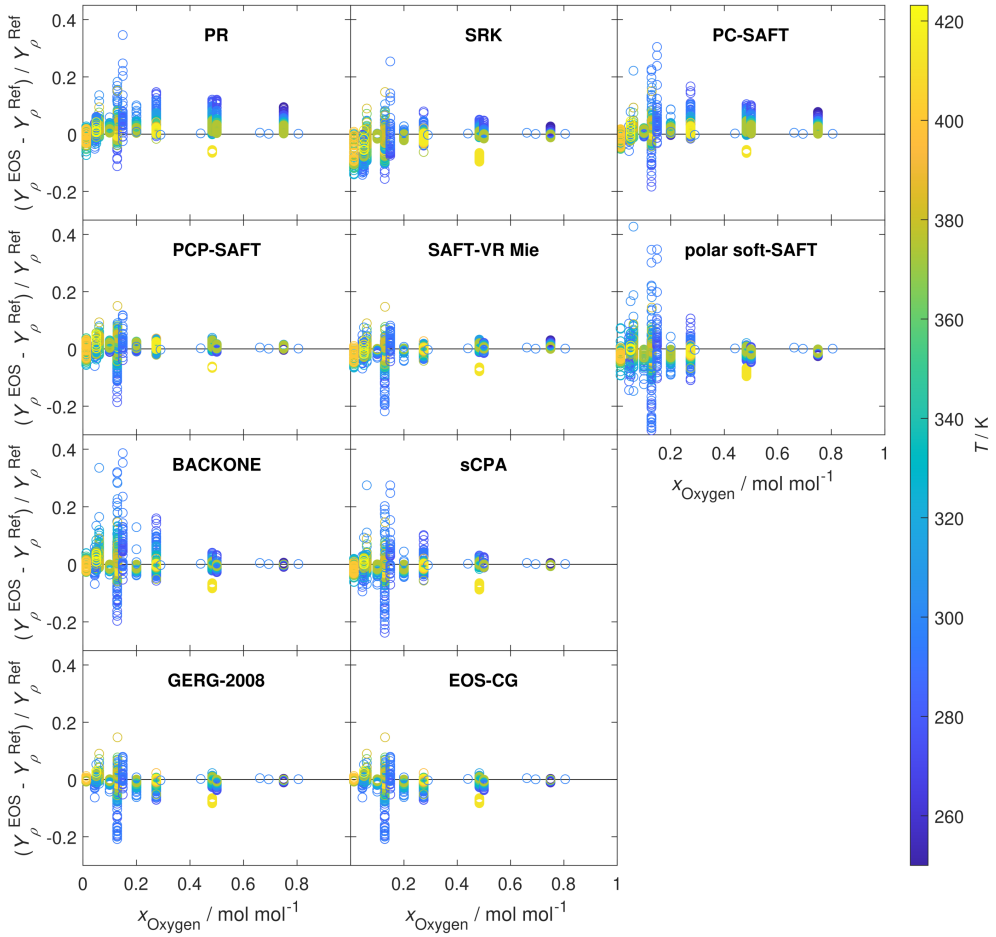

Fig. S4 Deviations between the experimental density data (Ref) [1, 31, 34–39] and calculated density by each of the ten studied EOS (predictive mode) [5, 9, 11, 13–22] of the binary $CO_2 + O_2$ mixture. The deviations are shown in dependency of the mole fraction of oxygen (O_2) and are colored by temperature according to the color bar on the right.

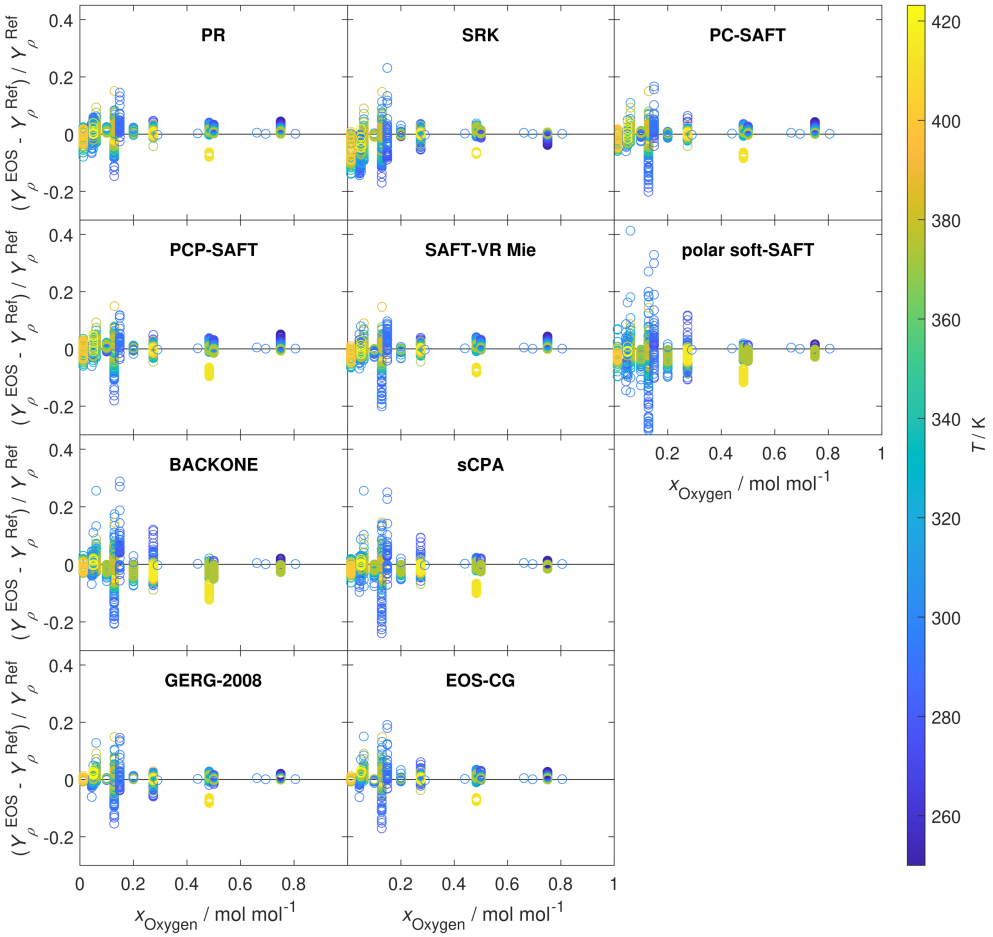

Fig. S5 Deviations between the experimental density data (Ref) [1, 31, 34–39] and calculated density by each of the ten studied EOS (adjusted mode) [5, 9, 11, 13–22] of the binary $CO_2 + O_2$ mixture. The deviations are shown in dependency of the mole fraction of oxygen (O_2) and are colored by temperature according to the color bar on the right.

References

[1] Mantovani, M., Chiesa, P., Valenti, G., Gatti, M., Consonni, S.: Supercritical pressure–density–temperature measurements on CO_2–N_2, CO_2–O_2 and CO_2–Ar binary mixtures. The Journal of Supercritical Fluids **61**, 34–43 (2012) https://doi.org/10.1016/j.supflu.2011.09.001

[2] Tsivintzelis, I., Kontogeorgis, G.M., Michelsen, M.L., Stenby, E.H.: Modeling phase equilibria for acid gas mixtures using the CPA equation of state. Part II: Binary mixtures with CO_2. Fluid Phase Equilibria **306**, 38–56 (2011) https://doi.org/10.1016/j.fluid.2011.02.006

[3] Sun, L., Liang, X., Solms, N., Kontogeorgis, G.M.: Solubility Modeling of Air in Aqueous Electrolyte Solutions with the e-CPA Equation of State. Industrial & Engineering Chemistry Research **59**(41), 18693–18704 (2020) https://doi.org/10.1021/acs.iecr.0c03164

[4] Diamantonis, N.I., Economou, I.G.: Evaluation of Statistical Associating Fluid Theory (SAFT) and Perturbed Chain-SAFT Equations of State for the Calculation of Thermodynamic Derivative Properties of Fluids Related to Carbon Capture and Sequestration. Energy & Fuels **25**, 3334–3343 (2011) https://doi.org/10.1021/ef200387p

[5] Gross, J.: An equation-of-state contribution for polar components: Quadrupolar molecules. AIChE Journal **51**, 2556–2568 (2005) https://doi.org/10.1002/aic.10502

[6] Dufal, S., Lafitte, T., Galindo, A., Jackson, G., Haslam, A.J.: Developing intermolecular-potential models for use with the SAFT-VR Mie equation of state. AIChE Journal **61**(9), 2891–2912 (2015) https://doi.org/10.1002/aic.14808

[7] Alkhatib, I.I.I., Llovell, F., Vega, L.F.: Assessing the effect of impurities on the thermophysical properties of methane-based energy systems using polar soft-SAFT. Fluid Phase Equilibria **527**, 112841 (2021) https://doi.org/10.1016/j.fluid.2020.112841

[8] Dias, A.M.A., Pàmies, J.C., Coutinho, J.a.A.P., Marrucho, I.M., Vega, L.F.: SAFT Modeling of the Solubility of Gases in Perfluoroalkanes. The Journal of Physical Chemistry B **108**, 1450–1457 (2004) https://doi.org/10.1021/jp036225o

[9] Müller, A., Winkelmann, J., Fischer, J.: Backone family of equations of state: 1. Nonpolar and polar pure fluids. AIChE Journal **42**, 1116–1126 (1996) https://doi.org/10.1002/aic.690420423

[10] Bell, I.H., Jäger, A.: Helmholtz Energy Transformations of Common Cubic Equations of State for Use with Pure Fluids and Mixtures. Journal of Research of the National Institute of Standards and Technology **121**, 238–263 (2016)

https://doi.org/10.6028/jres.121.011

[11] Kontogeorgis, G.M., Michelsen, M.L., Folas, G.K., Derawi, S., Solms, N., Stenby, E.H.: Ten Years with the CPA (Cubic-Plus-Association) Equation of State. Part 1. Pure Compounds and Self-Associating Systems. Industrial & Engineering Chemistry Research **45**(14), 4855–4868 (2006) https://doi.org/10.1021/ie051305v

[12] Müller, A., Winkelmann, J., Fischer, J.: BACKONE family of equations of state: 1. nonpolar and polar pure fluids. AIChE Journal **42**(4), 1116–1126 (1996) https://doi.org/10.1002/aic.690420423

[13] Weingerl, U., Wendland, M., Fischer, J., Müller, A., Winkelmann, J.: Backone family of equations of state: 2. nonpolar and polar fluid mixtures. AIChE Journal **47**(3), 705–717 (2001) https://doi.org/10.1002/aic.690470317

[14] Soave, G.: Equilibrium constants from a modified Redlich-Kwong equation of state. Chemical Engineering Science **27**(6), 1197–1203 (1972) https://doi.org/10.1016/0009-2509(72)80096-4

[15] Peng, D.-Y., Robinson, D.B.: A new two-constant equation of state. Industrial & Engineering Chemistry Fundamentals **15**(1), 59–64 (1976) https://doi.org/10.1021/i160057a011

[16] Gross, J., Sadowski, G.: Perturbed-Chain SAFT: An equation of state based on a perturbation theory for chain molecules. Industrial & Engineering Chemistry Research **40**(4), 1244 (2001) https://doi.org/10.1021/ie0003887

[17] Lafitte, T., Apostolakou, A., Avendaño, C., Galindo, A., Adjiman, C.S., Müller, E.A., Jackson, G.: Accurate statistical associating fluid theory for chain molecules formed from Mie segments. The Journal of Chemical Physics **139**, 154504 (2013) https://doi.org/10.1063/1.4819786

[18] Blas, F.J., Vega, L.F.: Thermodynamic behaviour of homonuclear and heteronuclear Lennard-Jones chains with association sites from simulation and theory. Molecular Physics **92**, 135–150 (1997) https://doi.org/10.1080/002689797170707

[19] Alkhatib, I.I.I., Pereira, L.M.C., Torne, J., Vega, L.F.: Polar soft-SAFT: theory and comparison with molecular simulations and experimental data of pure polar fluids. Phys. Chem. Chem. Phys. **22**, 13171–13191 (2020) https://doi.org/10.1039/D0CP00846J

[20] Kontogeorgis, G.M., V. Yakoumis, I., Meijer, H., Hendriks, E., Moorwood, T.: Multicomponent phase equilibrium calculations for water–methanol–alkane mixtures. Fluid Phase Equilibria **158-160**, 201–209 (1999) https://doi.org/10.1016/S0378-3812(99)00060-6

[21] Kunz, O., Wagner, W.: The GERG-2008 Wide-Range Equation of State for Natural Gases and Other Mixtures: An Expansion of GERG-2004. Journal of Chemical & Engineering Data **57**, 3032–3091 (2012) https://doi.org/10.1021/je300655b

[22] Gernert, J., Span, R.: EOS–CG: A Helmholtz energy mixture model for humid gases and CCS mixtures. The Journal of Chemical Thermodynamics **93**, 274–293 (2016) https://doi.org/10.1016/j.jct.2015.05.015

[23] Westman, S.F., Stang, H.G.J., Løvseth, S.W., Austegard, A., Snustad, I., Ertesvåg, I.S.: Vapor-liquid equilibrium data for the carbon dioxide and oxygen (CO_2 + O_2) system at the temperatures 218, 233, 253, 273, 288 and 298 K and pressures up to 14 MPa. Fluid Phase Equilibria **421**, 67–87 (2016) https://doi.org/10.1016/j.fluid.2016.04.002

[24] Fredenslund, A., Sather, G.: Gas-liquid equilibrium of the oxygen-carbon dioxide system. Journal of Chemical and Engineering Data **15**(1), 17–22 (1970) https://doi.org/10.1021/je60044a024

[25] Kaminishi, G.-I., Toriumi, T.: Gas-liquid equilibrium under high pressures. vi. vapor-liquid phase equilibrium in the CO_2-H_2, CO_2-N_2, and CO_2-O_2 systems. Journal of the Society of Chemical Industry, Japan **69**(2), 175–178 (1966) https://doi.org/10.1246/nikkashi1898.69.2_175

[26] Fredenslund, A., Jørgen, M., Persson, O.: Gas-liquid equilibrium of oxygen-carbon dioxide system. Journal of Chemical and Engineering Data **17**(4), 440–443 (1972) https://doi.org/10.1021/je60055a019

[27] Lasala, S., Chiesa, P., Privat, R., Jaubert, J.-N.: VLE properties of CO_2 – Based binary systems containing N_2, O_2 and Ar: Experimental measurements and modelling results with advanced cubic equations of state. Fluid Phase Equilibria **428**, 18–31 (2016) https://doi.org/10.1016/j.fluid.2016.05.015

[28] Belkadi, A., Hadj-Kali, M.K., Llovell, F., Gerbaud, V., Vega, L.F.: Soft-SAFT modeling of vapor–liquid equilibria of nitriles and their mixtures. Fluid Phase Equilibria **289**(2), 191–200 (2010) https://doi.org/10.1016/j.fluid.2009.12.012

[29] Zhu, C., Liu, X., Xue, S., He, M.: A Comprehensive Study on Thermophysical Properties of Carbon Dioxide through the Cubic-Plus-Association and Crossover Cubic-Plus-Association Equations of State. Journal of Chemical & Engineering Data **65**(9), 4268–4284 (2020) https://doi.org/10.1021/acs.jced.0c00236

[30] Bymaster, A., Emborsky, C., Dominik, A., Chapman, W.G.: Renormalization-Group Corrections to a Perturbed-Chain Statistical Associating Fluid Theory for Pure Fluids Near to and Far from the Critical Region. Industrial & Engineering Chemistry Research **47**(16), 6264–6274 (2008) https://doi.org/10.1021/ie8001167

[31] Al-Siyabi, I.: Effect of impurities on CO_2 stream properties. PhD thesis, Heriot-Watt University, United Kingdom (2013). https://doi.org/10399/2643

[32] Lin, C.-W., Trusler, J.P.M.: Speed of Sound in (Carbon Dioxide + Propane) and Derived Sound Speed of Pure Carbon Dioxide at Temperatures between (248 and 373) K and at Pressures up to 200 MPa. Journal of Chemical & Engineering Data **59**(12), 4099–4109 (2014) https://doi.org/10.1021/je5007407

[33] Gross, J., Sadowski, G.: Application of the perturbed-chain SAFT equation of state to associating systems. Industrial & Engineering Chemistry Research **41**(22), 5510–5515 (2002) https://doi.org/10.1021/ie010954d

[34] Lozano-Martín, D., Vega-Maza, D., Martín, M.C., Tuma, D., Chamorro, C.R.: Thermodynamic characterization of the (CO_2 + O_2) binary system for the development of models for CCS processes: Accurate experimental (p, ρ, T) data and virial coefficients. The Journal of Supercritical Fluids **169**, 105074 (2021) https://doi.org/10.1016/j.supflu.2020.105074

[35] Ahamada, S., Valtz, A., Chabab, S., Blanco-Martín, L., Coquelet, C.: Experimental Density Data of Three Carbon Dioxide and Oxygen Binary Mixtures at Temperatures from 276 to 416 K and at Pressures up to 20 MPa. Journal of Chemical & Engineering Data **65**, 5313–5327 (2020) https://doi.org/10.1021/acs.jced.0c00484

[36] Lozano-Martín, D., Akubue, G.U., Moreau, A., Tuma, D., Chamorro, C.R.: Accurate experimental (p, ρ, T) data of the (CO_2 + O_2) binary system for the development of models for CCS processes. The Journal of Chemical Thermodynamics **150**, 106210 (2020) https://doi.org/10.1016/j.jct.2020.106210

[37] Commodore, J.A., Deering, C.E., Marriott, R.A.: Volumetric properties and phase behavior of sulfur dioxide, carbon disulfide and oxygen in high-pressure carbon dioxide fluid. Fluid Phase Equilibria **477**, 30–39 (2018) https://doi.org/10.1016/j.fluid.2018.08.012

[38] Mazzoccoli, M., Bosio, B., Arato, E.: Pressure–Density–Temperature Measurements of Binary Mixtures Rich in CO_2 for Pipeline Transportation in the CCS Process. Journal of Chemical & Engineering Data **57**, 2774–2783 (2012) https://doi.org/10.1021/je300590v

[39] Gururaja, G.J., Tirunarayanan, M.A., Ramachandran, A.: Dynamic viscosity of gas mixtures. Journal of Chemical & Engineering Data **12**(4), 562–567 (1967) https://doi.org/10.1021/je60035a024